

Squeezing more out of 2D seismic data: Processing and interpretation of a pseudo-3D seismic survey from New Zealand

J. Helen Isaac and Don C. Lawton

ABSTRACT

During the acquisition of seismic data near Christchurch, New Zealand, in 2011, some receivers along a 2D line were left live to record data from sources located on an orthogonal 2D line. We created a pseudo-3D seismic survey from these data. We processed the data somewhat unconventionally to remove shot-generated noise and stacked it into bins having the same dimension as the receiver spacing in order to increase the fold. We interpreted faults on the pseudo-3D data and were able to update the regional fault trend interpreted previously using 2D data integrated with regional mapping.

INTRODUCTION

In 2011, CREWES acquired six seismic lines near the city of Christchurch, New Zealand, after a major earthquake in 2010 destroyed large parts of the city. The objective was to map faults to assist in hazard assessment. The faults interpreted from the seismic data integrated with regional knowledge of fault trends are shown in white on Figure 1 (from Lawton et al., 2011).

During the 2D seismic data acquisition, some receivers at the north end of Robinson's Road line (line 5) were kept live to record during the shooting of Newton's Road line (line 6), which is orthogonal (Figure 1), thus allowing us to create a small pseudo-3D survey. We processed the data and were able to interpret vertical discontinuities that suggested the presence of transverse faults.

DATA PROCESSING

During the data acquisition in 2011, 221 vibrator points from line 6, spaced 20 m apart, were shot into 120 receivers 10 m apart along orthogonal line 5. Noise observed in the data has velocity moveout ranging between 170 m/s and 550 m/s. The six representative shots displayed in Figure 2 show how the noise gets shallower in arrival time as the shots get closer to the receiver line and that there are several sources of noise.

We applied several noise attenuation procedures to the data to remove these undesired events. After much testing of sequences of processes, the final sequence chosen was that which gave the best results. Figures 3 to 6 show the improvement in the signal/noise ratio in the gathers as the processing progresses. All the data include the refraction statics supplied by Sensor from their processing of the 2D lines. The processes we applied include air blast attenuation and predictive deconvolution (Figure 3), further air blast attenuation on receiver gathers and a bandpass filter of 15-20-90-100 Hz (Figure 4), trace equalisation and Gabor deconvolution (Figure 5), and NMO correction, 5-trace mixing of NMO-corrected gathers, NMO removal and a bandpass filter of 5-10-90-100 Hz (Figure 6). Usually one would not expect to apply both predictive deconvolution and Gabor deconvolution or to mix NMO-corrected shot gathers but this non-standard processing

stream resulted in the greatest amount of noise attenuation and enhancement of the stacked data.

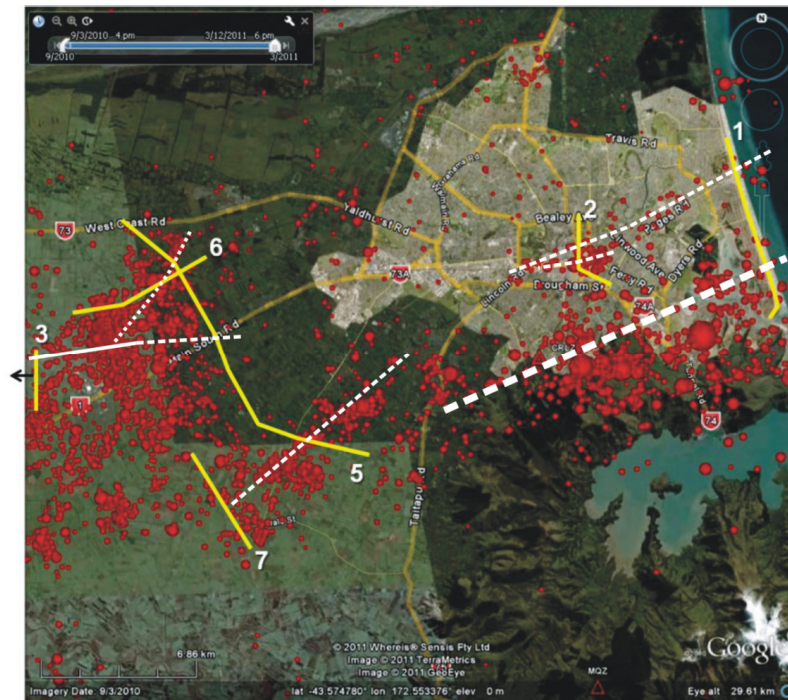


FIG. 1: Layout of the 2D seismic lines acquired near Christchurch with interpreted faults in white. The red dots show the epicentres of aftershocks as of June 2011 (GNS Science). Map data courtesy © 2011 Europa Technologies, © 2011 Google and © 2011 Whereis® Sensis Pty Ltd Imagery © 2011 NASA. We discuss data sourced along line 6 and recorded by some of the receivers on line 5 (from Lawton et al., 2011).

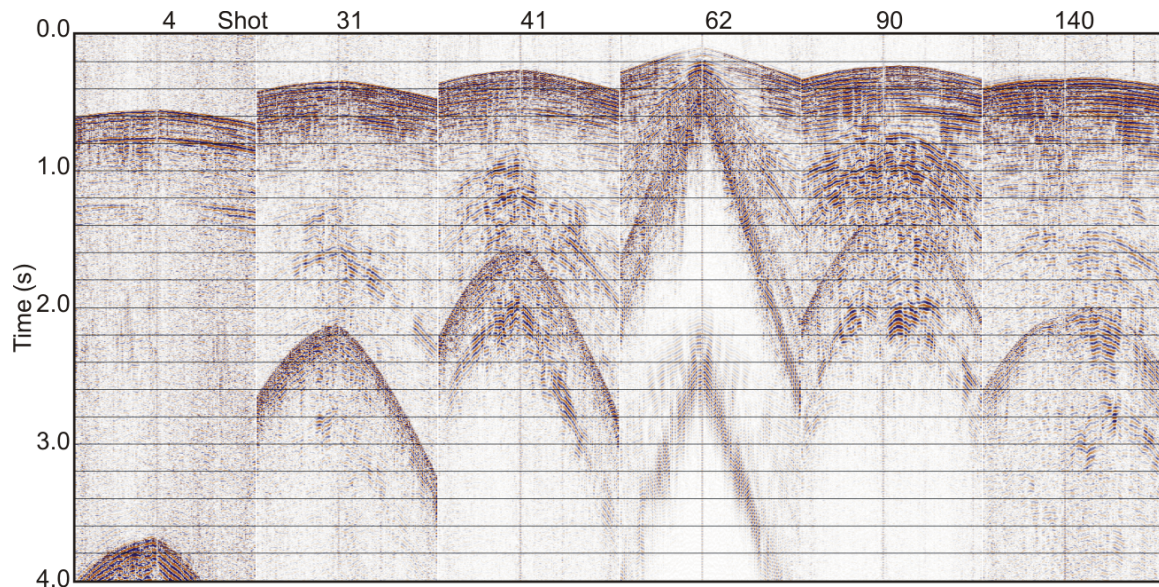


FIG. 2: Six representative shots showing different noise and how the noise gets shallower in time as the shots approach the receiver line.

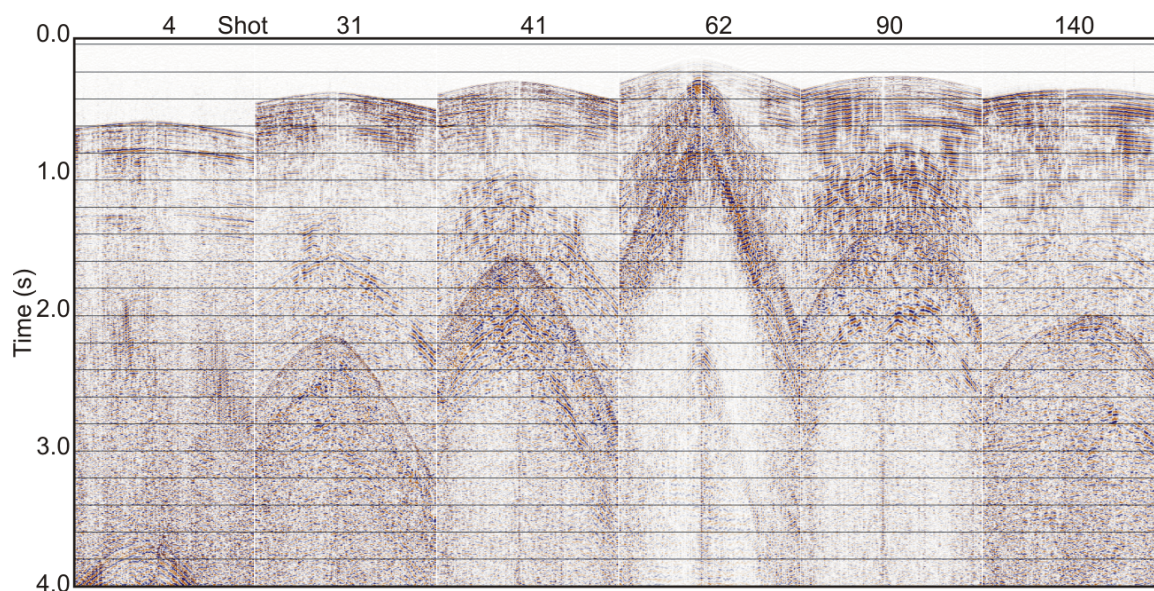


FIG. 3: The six shot gathers from Figure 2 after air blast attenuation and predictive deconvolution.

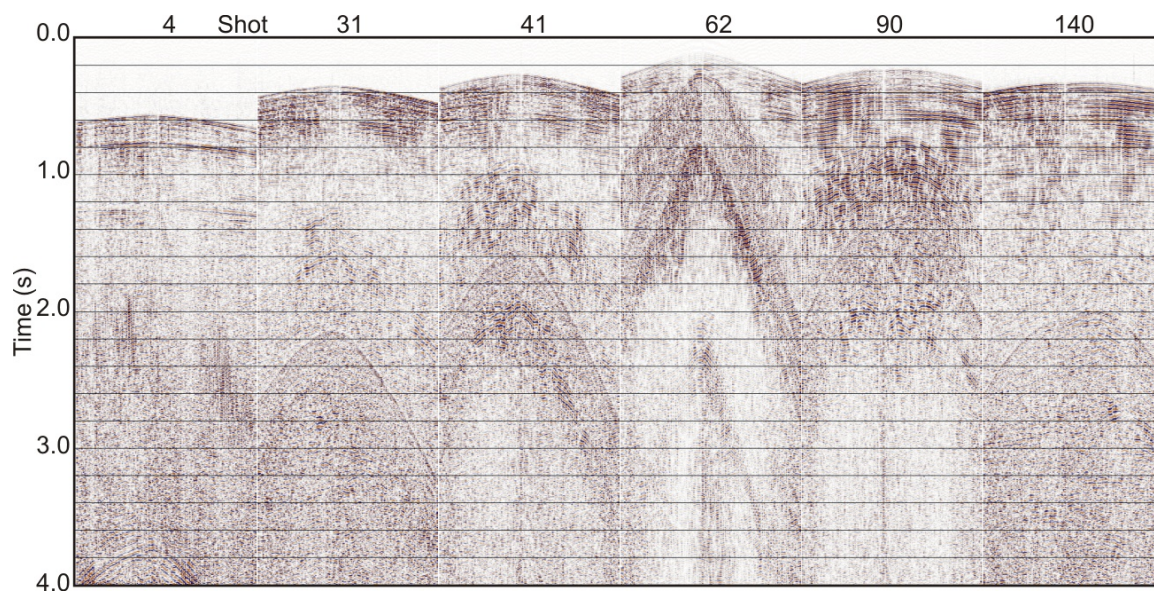


FIG. 4: The six shot gathers from Figure 3 after additional air blast attenuation on receiver gathers and bandpass filter of 15-20-90-100 Hz.

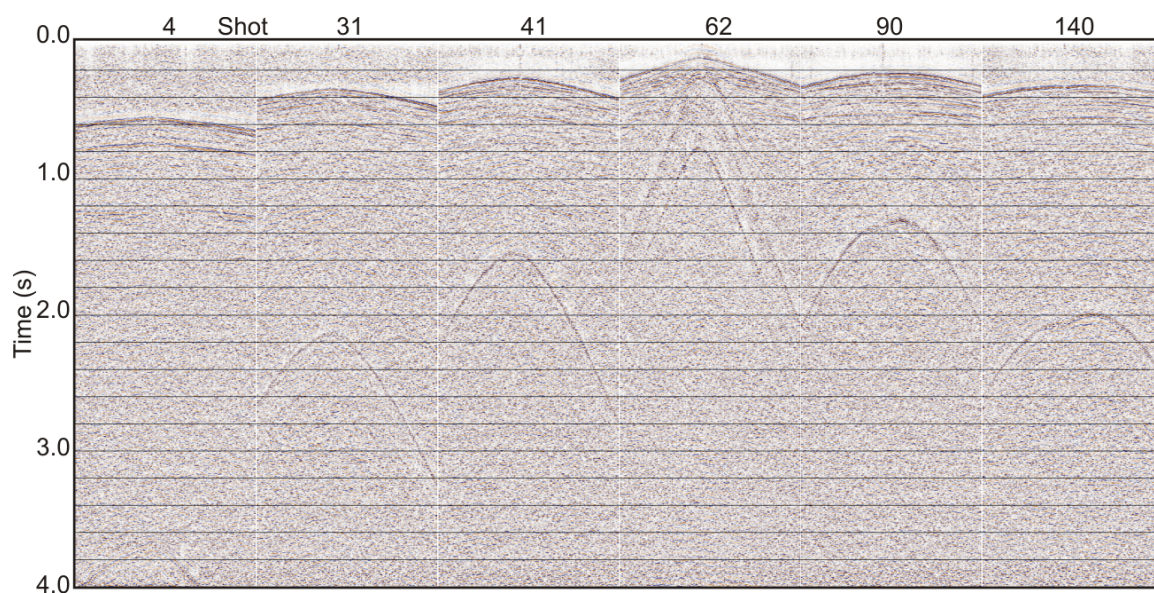


FIG. 5: The six shot gathers from Figure 4 after Gabor deconvolution.

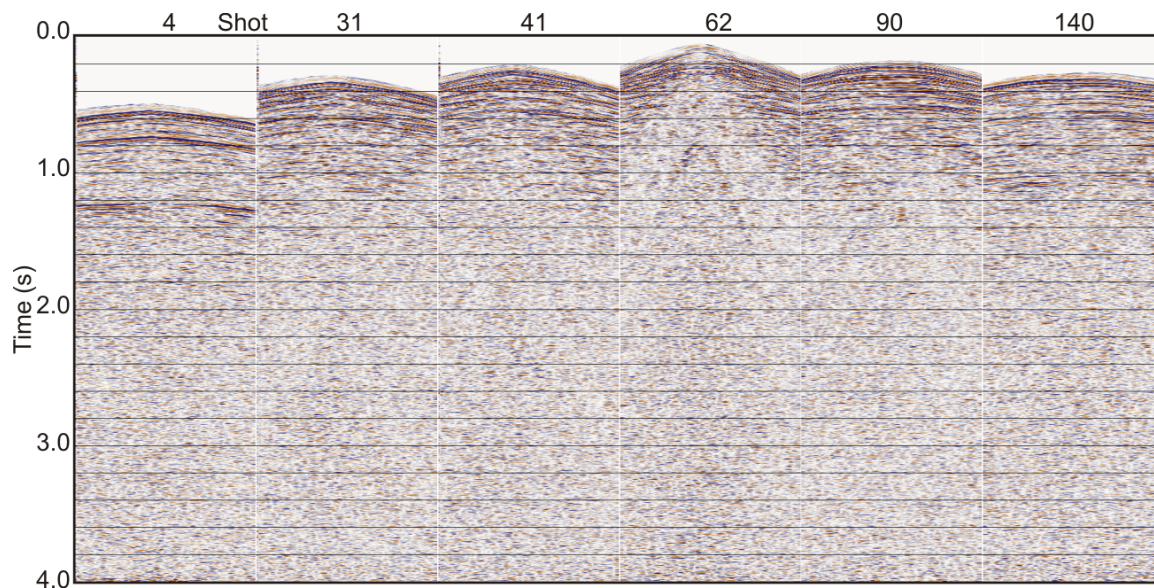


FIG. 6: The six shot gathers from Figure 5 after 5-trace mixing of NMO-corrected gathers, NMO removal and 5-10-90-100 Hz bandpass filter.

We 3D binned the data using a bin size of 10x10 m (Figure 7). This size was preferred over a standard 5x5 m bin size (half receiver spacing) as it increased the low CMP fold somewhat. The fold is greatest to the west of the receiver line, being between 6 and 13 over crosslines 67 to 86. Some CMP bins were empty so after application of NMO and stack we padded the dataset with blank traces then did a 3-trace mix to interpolate the blank traces with data from the two adjacent traces. Figure 8 shows a sample stacked inline before and after padding and trace mixing. After this procedure we post-stack migrated the data using a finite-difference algorithm, muted migration smiles and killed padded traces at the ends of the lines. The area covered by the pseudo-3D at a reflection time of 1 s is about 580x1420 m.

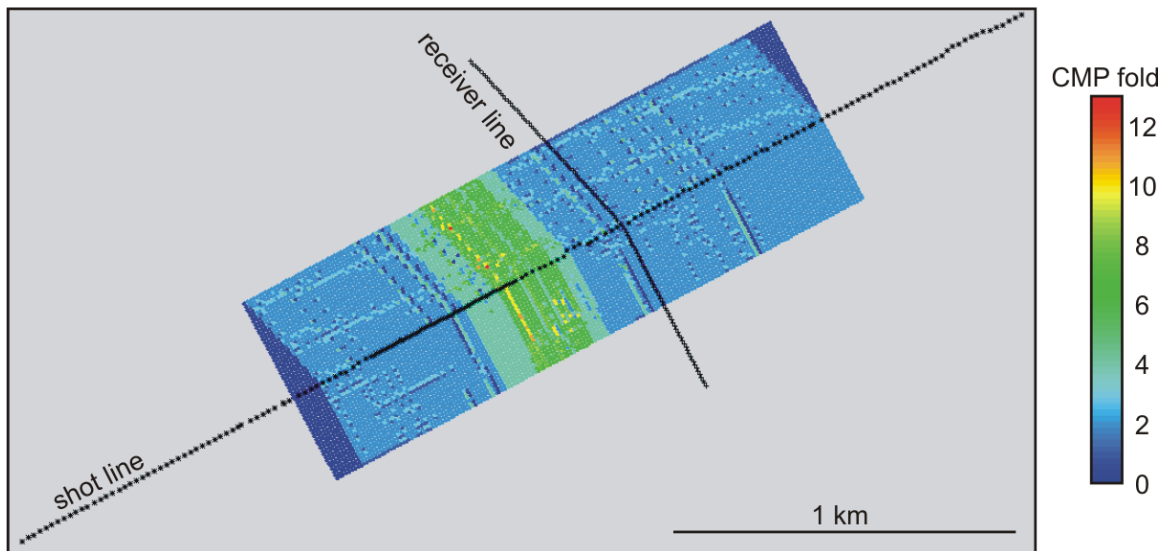


FIG. 7: Plot of CMP bin fold with shot and receiver lines.

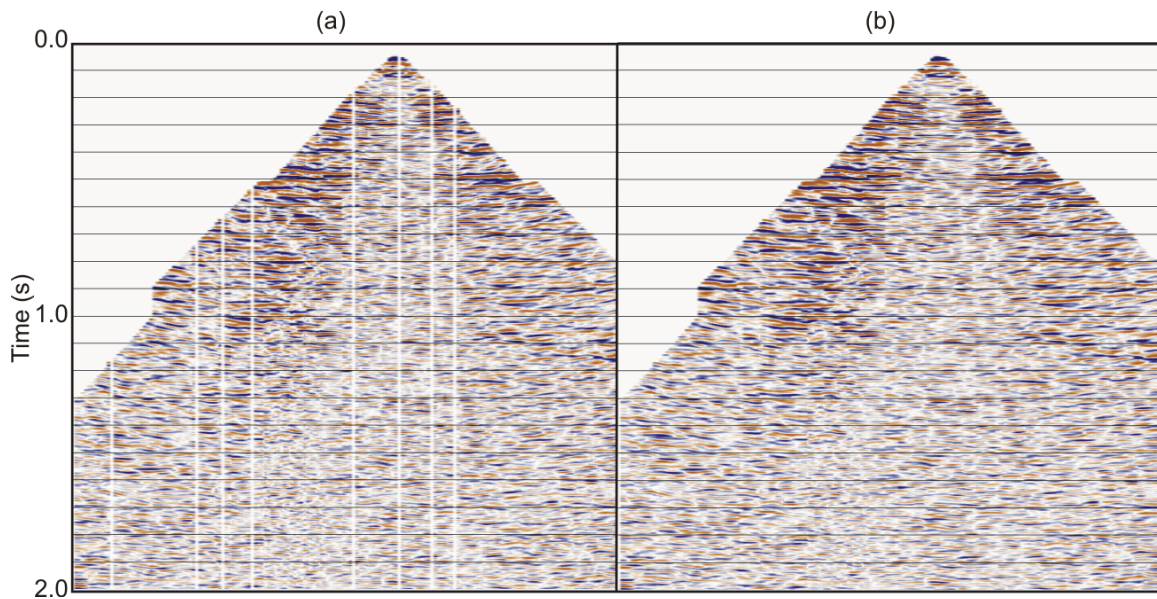


FIG. 8: Stacked Inline 30 before (a) and after (b) padding of empty CMP bins and 3-trace mix.

The migrated pseudo-3D and the 2D data processed by Sensor were imported into a Kingdom Suite project for interpretation. In Figure 9 we see three semi-parallel lines: crossline 77, Robinson's Road 2D line (line 5) from cdps 2700 to 2300, and crossline 146. The faults on Robinson's Road line were interpreted by Lawton et al. (2011) and the red fault on the crosslines is interpreted to be the same one as the red fault on Robinson's Road line. The map in Figure 9 shows the displayed lines and the trace of the red fault. Crossline 77 has fold of 6-9 thus is far more reliable than crossline 1467, which has fold of only 1-3. The trend of the red fault is in agreement with the interpreted fault crossing lines 5 and 6 that was shown on Figure 1. We have changed the direction of this fault slightly to reflect the fault trace interpreted on the pseudo-3D data (Figure 10).

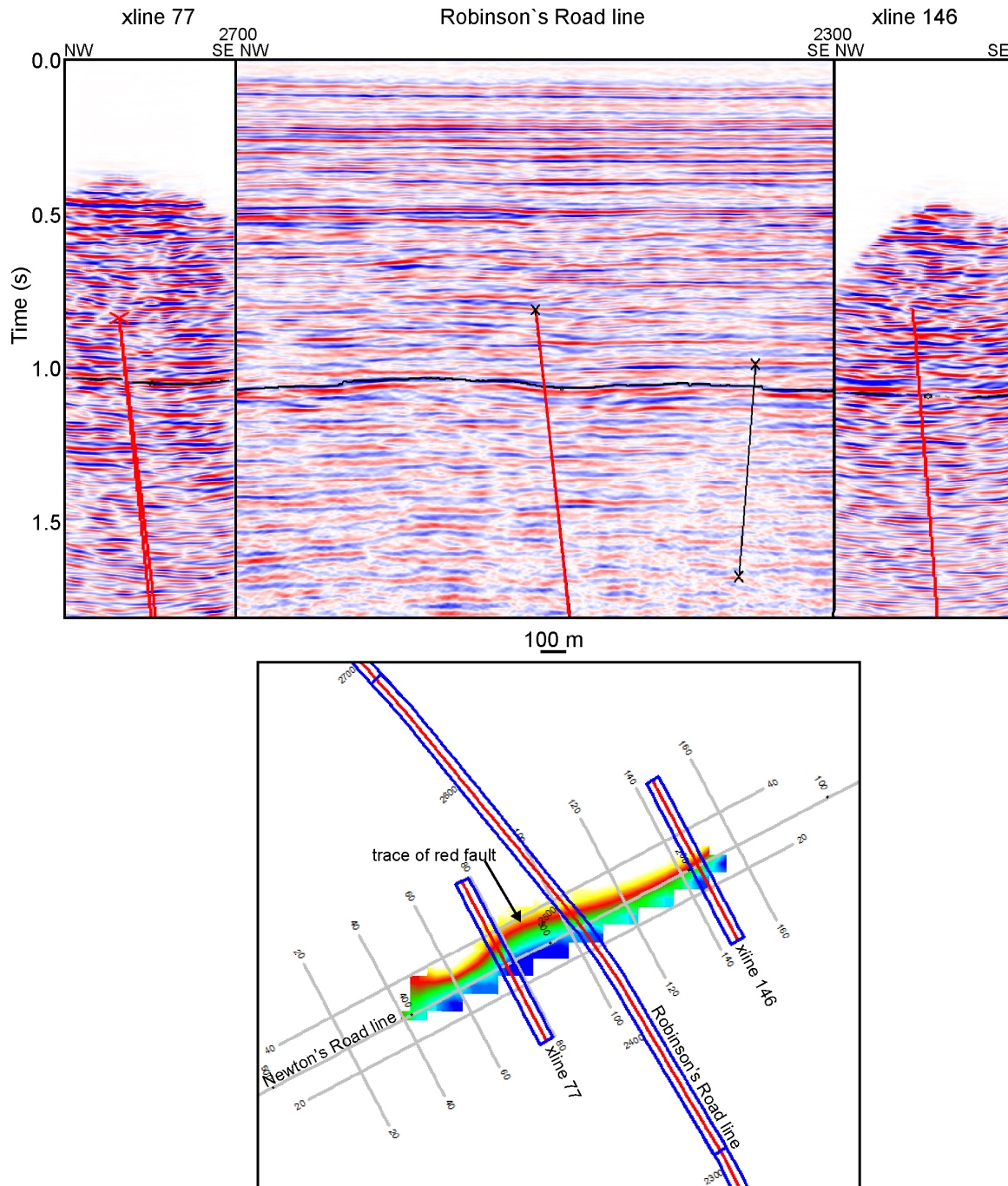


FIG. 9: Three semi-parallel lines: crossline 77, Robinson's Road 2D line from cdps 2700 to 2300 (from Lawton, 2011), and crossline 146. The red fault on the crosslines is interpreted to be the same one as the red fault interpreted previously (Lawton et al., 2011) on Robinson's Road line and its trace is displayed on the map.

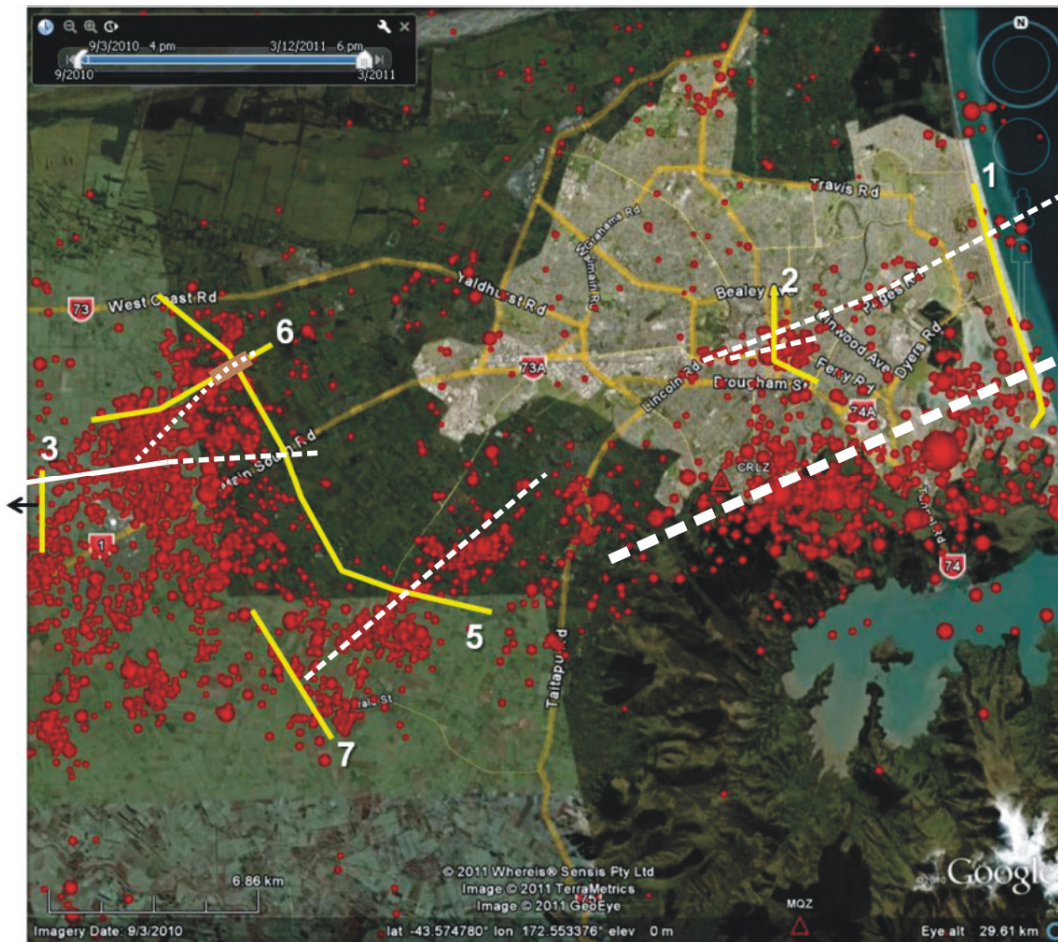


FIG 10: Map shown in Figure 1 with the adjusted trace of the fault cutting lines 5 and 6 based on the interpretation of the fault trace on the pseudo-3D survey (terracotta oblong).

CONCLUSIONS

By processing seismic data acquired by recording along a line orthogonal to a source line we were able to create a pseudo-3D seismic survey. Despite the low fold of the binned and stacked data, we were able to interpret a major fault on the pseudo-3D survey, to correlate this fault with one interpreted on the 2D surveys and to update the fault map.

ACKNOWLEDGEMENTS

We would like to thank the CREWES sponsors, the New Zealand Crisis Management Centre, the Institute of Geological and Nuclear Sciences, and the University of Canterbury. We thank Sensor Geophysical for data processing information, and Landmark and Kingdom Suite for software.

REFERENCES

- Google Earth, 2011, Google Earth version 6.0.3.2197 software downloaded and installed from <http://www.google.com/earth/index.html>, images accessed October 17, 2011.
- Lawton, D. C., M. B. Bertram, K. W. Hall, K. L. Bertram and J. Pettinga, 2011, Post-earthquake seismic reflection survey, Christchurch, New Zealand: CREWES Research Report vol. 23.